

Original paper

Ferraioloite from the Sítio do Castelo mine, Folgoso (Guarda, Portugal), description and Raman spectroscopy

Jaromír TVRDÝ^{1*}, Jiří SEJKORA², Pierre ROSSEEL³, Zdeněk DOLNÍČEK²¹ Department of Geology, Faculty of Science, Masaryk University, Kotlářská 267/2, CZ-61137 Brno, Czech Republic; jt.geologie@gmail.com² Department of Mineralogy and Petrology, National Museum, Cirkusová 1740, CZ-19300 Praha 9-Horní Počernice, Czech Republic³ Nazaret dreef 103, B-2500 Lier, Belgium

* Corresponding author



A zinc phosphate corresponding to ferraioloite with low Mg and high Na cation contents in interlayer space was identified in samples from the Sítio do Castelo mine, Folgoso (Guarda, Portugal). It occurs as sky-blue, pearly lustrous, radial or irregular aggregates up to 1 mm in size composed of very thin elongated flaky crystals. The mineral is monoclinic, space group $I2/m$, with unit-cell parameters refined from X-ray powder diffraction data: $a = 25.417(7)$, $b = 6.342(4)$, $c = 15.186(5)$ Å, $\beta = 90.02(4)^\circ$, $V = 2448.0(17)$ Å³. The chemical composition generally agrees with published data for ferraioloite, but differs significantly in elements present at sites assumed to be in the interlayer of the crystal structure. The corresponding empirical formula based on 8 (PO)₄ and 4 (OH) groups *pfu* is $(\text{Mg}_{0.16}\text{Na}_{0.15}\text{Ca}_{0.09}\text{K}_{0.01})_{\Sigma 0.41}\text{Mn}_{4.22}(\text{Fe}^{2+}_{1.64}\text{Fe}^{3+}_{1.15}\text{Al}_{1.47})_{\Sigma 4.26}\text{Zn}_{3.87}(\text{PO}_4)_8(\text{OH})_4(\text{H}_2\text{O})_{20}$. The Raman spectra and tentative assignment of observed bands are given. The most prominent bands are attributed to stretching and bending vibrations of phosphate tetrahedra and complex metal-centered polyhedra. Bands of O–H stretching vibrations are weak, and bending vibrations of water molecules were not observed. The origin of the mineral is related to in-situ supergene weathering of zwieselite–triplite and isokite–fluorapatite assemblages with admixtures of sphalerite.

Keywords: ferraioloite, powder X-ray diffraction, chemical composition, Raman spectroscopy, supergene weathering

Received: 10 April 2021; **accepted:** 15 September 2021; **handling editor:** R. Skála

1. Introduction

Ferraioloite, ideally $\text{MgMn}^{2+}_4(\text{Fe}^{2+}_{0.5}\text{Al}^{3+}_{0.5})_4\text{Zn}_4(\text{PO}_4)_8(\text{OH})_4(\text{H}_2\text{O})_{20}$, was described as a new mineral by Mills et al. (2016) from the Foote Lithium Company mine, Kings Mountain district (North Carolina, USA), a pegmatite locality well known for a variety of rare phosphates and silicates. Structurally and chemically, ferraioloite is related to falsterite, $\text{Ca}_2\text{MgMn}^{2+}_2(\text{Fe}^{2+}_{0.5}\text{Fe}^{3+}_{0.5})_4\text{Zn}_4(\text{PO}_4)_8(\text{OH})_4(\text{H}_2\text{O})_{14}$ (Kampf et al. 2012). Both have a complex layer structure consisting of thick heteropolyhedral slabs bridged either by dimers of MgO_6 octahedra (in falsterite) or by hydrogen-bonded isolated $\text{Mg}(\text{H}_2\text{O})_6$ octahedra (in ferraioloite). During the study of secondary phosphates from Sítio do Castelo mine, Folgoso (Guarda, Portugal), a mineral phase corresponding to ferraioloite was confirmed by powder X-ray diffraction and chemical electron microprobe (EMP) analysis.

2. Occurrence

The Sítio do Castelo mine is located in the Serra da Estrela National Park in central Portugal, in the valley of the Freixo stream, about 500 m east of the center of

the medieval Folgoso village (40.511389, -7.508056). The first mining works date to 1917 when a wolframite-(cassiterite?)-bearing quartz lens was exploited. After World War II, the mine was closed due to decreased metal prices. It was reopened by a small wall quarry in 1976 and exploited for quartz raw material used for metallic silicon production until 1986. In 1998, the mine was declared officially “extinct” (Alves et al. 2016).

The previously mined W–(Sn) ores probably occurred in isolated quartz veins at several small mines in the surrounding area. According to Teixeira et al. (1967), the thickness of these veins ranges from 0.15 to 0.80 m. In the Sítio do Castelo mine, the ore mineralization was followed by a system of short (no more than 150 m) galleries extending upslope more than 50 meters above the quarry level. The relationship between these veins and the main quartz body exposed in the mine is not entirely clear. The main quartz body is about 5 m thick and steeply penetrates migmatitized schists. It is considered to be either the core of a large pegmatite body (pers. comm. A. Lima 2021) or a high-temperature hydrothermal vein accompanied by greisenization with the local presence of andalusite, garnet and gahnite (Garate-Olabe et al. 2012).

Irregular phosphate accumulations and sulphide aggregates (pyrite >> arsenopyrite >> chalcopyrite >>

sphalerite) occur frequently in the main body. Primary phosphates are represented predominantly by zwieselite–triplite and less commonly by isokite with admixed fluorapatite. Intense weathering yielded varied secondary phosphate assemblages, which differ concerning their source mineral. Related to alteration of zwieselite–triplite, there is an assemblage, which includes phosphosiderite, strengite, rockbridgeite–frondelite, cacoxenite, bermanite, beraunite, strunzite, stewartite, laueite, leucophosphite, benyacarite, fluorapatite, wavellite and kidwellite. Related to the alteration of triplite–zwieselite in association with fluorapatite and isokite, there is an assemblage, which includes ludlamite, vivianite, strunzite–zincstrunzite, Zn-rich rockbridgeite–frondelite, Mn-rich phosphophyllite, hydroxylapatite, jahnsite-(CaMnFe), earlshannonite, lun’okite and plimerite (Alves et al. 2012; Kampf et al. 2017). Ferraioloite reported herein occurs in the latter assemblage.

3. Sample description

Ferraioloite occurs in fissures at the contact of brownish resinous massive zwieselite–triplite with fine-grained grey isokite with admixed fluorapatite and sphalerite. The walls of the fissures are rimmed by abundant muscovite blades up to 1 mm in size.

The mineral forms very thin, elongated, irregular flakes up to 0.25 mm in length arranged in fan-shaped to lamellar aggregates (Fig. 1). The flakes are pale blue and transparent, with pearly luster and pale blue streak. They are flexible and show irregular fracture and perfect cleavage on $\{010\}$. Because of its pale blue color, the ferraioloite described here visually resembles the related

Zn-phosphate falsterite, rather than known samples of ferraioloite.

Minerals associated with ferraioloite include vivianite–metavivianite, earlshannonite–whitmoreite, jahnsite–keckite, strunzite–zincstrunzite, very rare lun’okite and several unspecified secondary phosphates. Ferraioloite was found by one of the authors (PR) in 2017 and 2018, and no samples have been found since.

The studied sample is deposited in the collections of the Department of Mineralogy and Petrology of the National Museum in Prague, Czech Republic, under the catalog number P1P 10/2021.

4. Chemical composition

The sample was analyzed with a Cameca SX-100 electron microprobe (National Museum, Prague) operated in the wavelength-dispersive mode with an accelerating voltage of 15 kV, a specimen current of 5 nA, and a beam diameter of 3–5 μm . The following lines and standards were used: K_{α} : albite (Na), BN (N), celestine (S), chalcocopyrite (Cu), Co (Co), Cr_2O_3 (Cr), diopside (Mg), fluorapatite (Ca, P), halite (Cl), hematite (Fe), LiF (F), Ni (Ni), rhodonite (Mn), sanidine (Al, K, Si), TiO_2 (Ti), vanadinite (V), ZnO (Zn); L_{α} : baryte (Ba), clinoclase (As), scheelite (W), Sn (Sn), wulfenite (Mo), YVO_4 (Y); L_{β} : celestine (Sr); M_{α} : bismuth (Bi), Th (Th), UO_2 (U) and wulfenite (Pb). Peak counting times (CT) were 20 s for all elements except for N, for which it was 100 s; CT for each background was one-half of the peak counting time. The raw intensities were converted to the concentrations automatically using the *PAP* (Pouchou and Pichoir 1985) matrix-correction procedure. The contents of As, Ba, Bi, Cl, Co, Cr, Cu, F, Mo, N, Pb, S, Si, Sn, Sr, Ti, Th, U, V, W and Y always were found to be below the detection limit (ca. 0.04–0.20 wt. %). Water content could not be analyzed directly because of the minute amount of material available. The H_2O content was confirmed by Raman spectroscopy and calculated based on the stoichiometry of the ideal formula. To maintain the charge balance and the number of (OH) equal to 4 *apfu*, both valence states of iron have been considered. The



Fig. 1 Pale blue radial aggregates of leafy crystals of ferraioloite from the Sítio do Castelo mine. FOV 0.8 mm. Photo J. Sejkora.

Tab. 1 Chemical composition of ferraioloite from the Sítio do Castelo mine (wt. %)

	Mean	Range	SD
Na ₂ O	0.26	0.12–0.60	0.16
K ₂ O	0.03	0.00–0.08	0.03
CaO	0.28	0.20–0.48	0.08
FeO	6.56	5.38–7.93	0.95
MgO	0.35	0.27–0.45	0.05
MnO	16.70	15.63–17.65	0.63
ZnO	17.56	16.37–18.16	0.54
Fe ₂ O ₃	5.13	3.04–6.87	1.15
Al ₂ O ₃	4.19	3.48–5.10	0.49
P ₂ O ₅	31.66	29.25–33.81	1.17
H ₂ O*	22.10		
Total	104.82		

Mean and range of 9 analyses; SD – standard deviation; H₂O* – H₂O content calculated based on the theoretical assumed content of 20 H₂O + 4 OH; Fe²⁺/Fe³⁺ ratio was inferred from the charge-balance.

presence of iron(III) is indirectly indicated by the blue color of the mineral, which was noted as indicative for Fe²⁺–Fe³⁺ charge transfer both in falsterite and ferraioloite (Kampf et al. 2012; Mills et al. 2016).

The analytical data are given in Tab. 1. The chemical composition and stoichiometry of the studied sample generally agree with the ideal formula of ferraioloite MgMn²⁺₄(Fe²⁺_{0.5}Al³⁺_{0.5})₄Zn₄(PO₄)₈(OH)₄(H₂O)₂₀. The main difference is in its content of Mg, the main cation in the interlayer, which is reported as 0.50 *apfu* in the holotype and found to be only 0.16 *apfu* in the studied sample. The empirical formula of ferraioloite from the Sítio do Castelo mine (mean of 9 analyses) on the basis of P = 8 *apfu* and (OH) = 4 is (Mg_{0.16}Na_{0.15}Ca_{0.09}K_{0.01})_{Σ0.41}Mn_{4.22}(Fe²⁺_{1.64}Fe³⁺_{1.15}Al_{1.47})_{Σ4.26}Zn_{3.87}(PO₄)₈(OH)₄(H₂O)₂₀.

Considering substitutions reported for structurally related layered Zn-phosphates (i.e., Kampf et al. 2012; Grey et al. 2018), a general chemical formula Mg(M1)₄(M2)₄Zn₄(PO₄)₈(OH)₄(H₂O)_x can be derived for both ferraioloite and falsterite, where M1 and M2 always represent two structural sites. In ferraioloite, M1 = Mn²⁺, M2 = Fe²⁺_{0.5}Al³⁺_{0.5}, x = 20, and in falsterite, M1 = Ca_{0.5}Mn²⁺_{0.5}, M2 = Fe²⁺_{0.5}Fe³⁺_{0.5}, x = 14. In these ideal formulas, Mg atoms occupy the interlayer and the remaining metals belong to the heteropolyhedral layer of atoms.

In the studied ferraioloite, 0.16 *apfu* Mg was found only. Other interlayer constituents must compensate for this deficiency, or the structure would undoubtedly contract in the c direction, which was not observed. The primary candidates

to be accommodated in the interlayer space are Na, Ca and K; the resulting interlayer cation content is most likely (Mg_{0.16}Na_{0.15}Ca_{0.09}K_{0.01})_{Σ0.41}. While Mg remains the dominant cation, it is almost equaled by Na and significantly exceeded by the total large-cation content. Almost identical content of large cations (0.21 *apfu* Ca) is reported by Mills et al. (2016) in the original sample of ferraioloite, but without specification of its position in the crystal structure, its structural role, and without comments to an excess of the sum of metal atoms considered to be in heteropolyhedral sites. In falsterite (Kampf et al. 2012), the role of Ca in the structure is different (Tab. 2).

The structural analysis could help solve this problem, but unfortunately, no reliable single-crystal X-ray diffraction data are available because the mineral occurs as parallel intergrowths of very thin flakes.

5. X-ray diffraction

Powder X-ray diffraction data were collected on a Bruker D8 Advance diffractometer (National Museum, Prague) with a solid-state 1D LynxEye detector (width 2.05°) using CuK_α radiation and operating at 40 kV and 40 mA. The powder pattern was collected using Bragg–Brentano geometry in the range 3–70° 2θ, in 0.01° steps with a counting time of 30 s per step. Positions and intensities of reflections were found and refined using the Pearson-VII profile-shape function with the ZDS program package (Ondruš 1993) and the unit-cell parameters were refined by the least-squares algorithm implemented by Burnham (1962). The experimental powder pattern was indexed in line with the calculated values of intensities obtained by the Lazy Pulverix program (Yvon et al. 1977) from the crystal structure of ferraioloite (Mills et al. 2016).

The experimental powder data given in Tab. 3 agree well with the data published for this mineral from the original locality (Mills et al. 2016) and with the X-ray pattern calculated from the structure of ferraioloite; experimental intensities are partly affected by the preferred orientation

Tab. 2 Tentative site occupations in ferraioloite and falsterite, assuming presence of large cations in the interlayer space of ferraioloite

Ferraioloite				Falsterite			
Ideally	Sample from Sítio do Castelo mine (current study)	Foote mine, USA (Mills et al. 2016)	Ideally	Palermo #1, USA (Kampf et al. 2012)			
Interlayer cations (<i>apfu</i>)							
Mg ²⁺	Mg ²⁺ _{0.16}	0.16	Mg ²⁺ _{0.50}	0.50	Mg ²⁺	Mg ²⁺ _{0.94} Zn ²⁺ _{0.06}	1.00
–	Na ⁺ _{0.15} Ca ²⁺ _{0.09} K ⁺ _{0.01}	0.25	Ca ²⁺ _{0.21}	0.21	–	–	–
	Σ	0.41	Σ	0.71	Σ	Σ	1.00
Heteropolyhedral layer atoms (<i>apfu</i>)							
Mn ²⁺ ₄	Mn ²⁺ _{4.22}	4.22	Mn ²⁺ _{4.16}	4.16	Ca ²⁺ ₂ Mn ²⁺ ₂	Ca ²⁺ _{2.02} Mn ²⁺ _{2.04}	4.06
Fe ²⁺ ₂ Al ³⁺ ₂	Fe ²⁺ _{1.64} Fe ³⁺ _{1.15} Al _{1.47}	4.26	Fe ²⁺ _{2.05} Al _{2.01}	4.06	Fe ²⁺ ₂ Fe ³⁺ ₂	Fe ²⁺ _{1.99} Fe ³⁺ _{1.99} Al ³⁺ _{0.01}	3.99
Zn ²⁺ ₄	Zn ²⁺ _{3.87}	3.87	Zn _{4.27}	4.27	Zn ²⁺ ₄	Zn ²⁺ _{4.00}	4.00
	Σ	12.35	Σ	12.49	Σ	Σ	12.05

Tab. 3 X-ray powder diffraction data for ferraioloite from the Sítio do Castelo Mine

<i>h</i>	<i>k</i>	<i>l</i>	<i>d</i> _{calc.}	Sítio do Castelo mine (this paper) Foote mine, USA (Mills et al. 2016)				
				<i>d</i> _{obs.}	<i>I</i> _{obs.}	<i>d</i> _{obs.}	<i>I</i> _{obs.}	<i>I</i> _{obs.}
2	0	0	12.709	12.707	100.0	12.7	100	
0	0	2	7.593	7.596	0.6	7.58	1	
4	0	0	6.354	6.356	1.0			
1	0	3	4.964	}	4.962	0.3	4.95	1
1	0	-3	4.965					
5	0	-1	4.821		4.832	0.1		
1	1	-2	4.781	}	4.783	0.3	4.78	4
1	1	2	4.781					
3	0	-3	4.346	}	4.334	0.1	4.33	1
3	0	3	4.345					
6	0	0	4.236		4.237	3.0	4.22	4
6	0	-2	3.700	}	3.699	0.8	3.699	3
6	0	2	3.699					
5	0	3	3.586		3.592	0.2	3.580	4
5	1	-2	3.516	}	3.519	0.5	3.499	5
5	1	2	3.515					
1	1	-4	3.231		3.230	0.2	3.245	7
1	0	-5	3.016	}	3.018	0.9	3.000	1
1	0	5	3.016					
8	0	-2	2.931		2.931	0.5	2.924	8
3	0	-5	2.859	}	2.862	0.3	2.869	5
3	0	5	2.859					
7	0	-4	2.624		2.624	1.3	2.616	4
10	1	1	2.3313		2.3324	0.1	2.352	2
12	0	0	2.1181		2.1209	0.1	2.113	2
6	2	4	2.1101		2.1063	0.1		
9	2	-1	2.0890		2.0879	0.1	2.083	2
0	0	8	1.8982		1.8971	0.2	1.8942	2
2	3	5	1.7191		1.7203	0.3		
15	0	-1	1.6841	}	1.6832	0.1		
15	0	1	1.6840					

as well as by the small amount material available for the study. The experimental pattern is distinctly different from the data published for chemically similar falsterite (Kampf et al. 2012) and jasonsmithite (Kampf et al. 2021). The refined unit-cell parameters of the studied sample (Tab. 4) are comparable with the published data (Mills et al. 2016).

6. Raman spectroscopy

The Raman spectra of the studied sample were collected in the range 4000–50 cm⁻¹ using a DXR dispersive

Tab. 4 Unit-cell parameters for ferraioloite (monoclinic space group *I2/m*)

	This paper		Mills et al. (2016)
	Powder XRD	Powder XRD	Single-crystal XRD
<i>a</i> [Å]	25.417(7)	25.320(6)	25.333(3)
<i>b</i> [Å]	6.342(4)	6.345(6)	6.299(1)
<i>c</i> [Å]	15.186(5)	15.267(6)	15.161(3)
β [°]	90.02(4)	91.031(5)	90.93(3)
<i>V</i> [Å ³]	2448.0(17)	2452.4(4)	2419.0(2)

Raman Spectrometer (Thermo Scientific) mounted on a confocal Olympus microscope. The Raman signal was excited by an unpolarised 633 nm He–Ne gas laser and detected by a CCD detector (size 1650 × 200 pixels, Peltier-cooled to -60 °C, quantum efficiency of 50 % and dynamic range 360–1100 nm). The experimental parameters were: 100× objective, 10 s exposure time, accumulation of 100 exposures, 25 μm pinhole spectrograph aperture, 2 mW laser power level, grating 400 per mm (estimated resolution 6.4–13.3 cm⁻¹). The spectra were repeatedly acquired from different grains to obtain a representative spectrum with the best signal-to-noise ratio. The possible thermal damage of the measured point was assessed by visual inspection of the exposed surface after measurement, observing possible decay of spectral features at the start of excitation and checking for thermal downshift of Raman lines. The instrument was set up by a software-controlled calibration procedure using multiple

neon emission lines (wavelength calibration), multiple polystyrene Raman bands (laser-frequency calibration) and standardized white-light sources (intensity calibration).

Spectral manipulations were performed using the Omnic 9 software (Thermo Scientific). Gaussian/Lorentzian (pseudo-Voigt) profile functions of the band-shape were used to obtain decomposed band components of the spectra. The decomposition was based on minimizing the difference in the observed and calculated profiles until the squared correlation coefficient (*r*²) was greater than 0.995.

To our knowledge, vibration spectra for ferraioloite have not yet been published. According to Mills et al. (2016), the mineral has a heteropolyhedral layer structure, with layers parallel to (100). The slabs consist of [Mn²⁺₄(Fe²⁺_{0.5}Al³⁺_{0.5})₄Zn₄(PO₄)₈(OH)₄(H₂O)₈] units built by (i) chains of pentamers formed by edge-shared dimers of [(Fe,Al)O₆] and [(Fe,Al)O₄(OH)₂] octahedra with wedged [MnO₄(H₂O)₂] octahedra, and (ii) parallel chains of edge-shared [ZnO₄] tetrahedra, both linked by [PO₄] tetrahedra

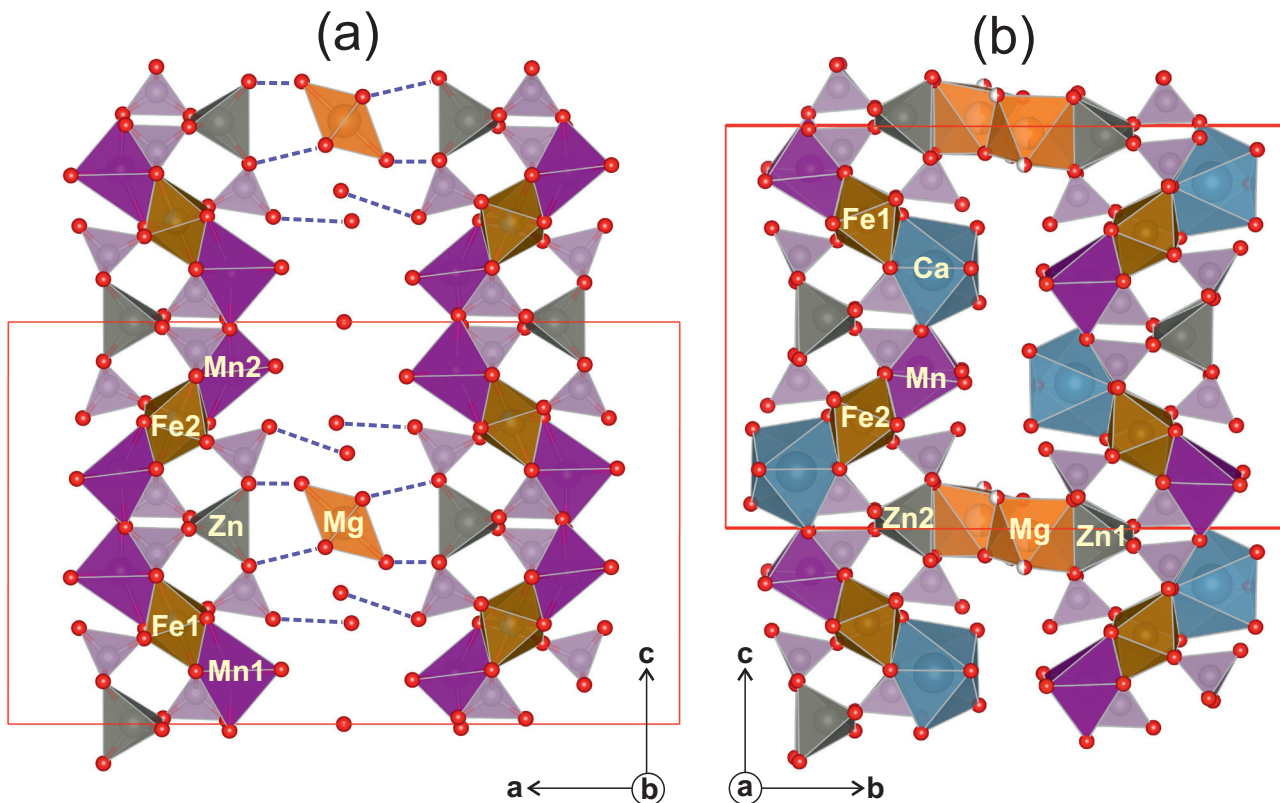


Fig. 2 Projections of the layered crystal structure of ferraioloite (a) and falsterite (b) according to data of Mills et al. (2016) and Kampf et al. (2012). Atoms of adjacent layers are omitted. Dashed lines correspond to hydrogen bonds between interlayer water molecules and layer oxygen atoms in ferraioloite.

(Fig. 2). The anions forming shared edges between the Mn-centred and Fe-centred octahedra are hydroxyl ions, and the unshared vertices of the Mn-centred octahedra are water molecules. The hydroxyl ions are partly deprotonated, maintaining a charge balance of the $\text{Fe}^{2+}\text{-Al}^{3+}$ heterovalent exchange. Isolated $[\text{Mg}(\text{H}_2\text{O})_6]$ octahedra, packing water molecules and most probably also Ca and/or Na are located in the interlayer. The cohesion is maintained by hydrogen bonding between the water molecules and oxygen acceptors.

According to Nakamoto (2009), octahedral units XY_6 exhibit six normal modes of vibration. Three of them are Raman active, ν_1 (A_{1g}) and ν_2 (E_g) stretching vibrations and ν_5 (F_{2g}) bending vibration. Tetrahedral XY_4 units with T_d symmetry have four normal modes of vibration, all Raman-active: ν_1 (A_1) symmetric stretching vibration, ν_2 (δ) (E) doubly degenerate bending vibration, ν_3 (F_2) triply degenerate antisymmetric stretching vibration, and ν_4 (δ) (F_2) triply degenerate bending vibration. In the crystalline state, deformation of polyhedra and lowering of symmetry leads to splitting of degenerate vibrations. Due to longer bond distances (from 1.942 Å for Zn–O up to 2.273 Å for Mn–O; Mills et al. 2016), stretching and bending $M\text{-O}$ vibrations are manifested in the region of low wavelengths, where they overlap with PO_4 vibrations.

The experimental Raman spectrum of the studied sample from the Sítio do Castelo mine (Fig. 3) is in general similar to that of other hydrated hydroxyphosphates. Tentative band assignments are given in Tab. 5.

The spectrum over the range 3800–2800 cm^{-1} is shown in Fig. 4a. As indicated by Chukanov and Vignasina (2020), Raman spectroscopy has a low sensitivity in the determination of water in minerals due to a weak response to excitation radiation. Bands of O–H stretching vibrations are usually observed in the range from 3800 to 3000 cm^{-1} , but bands of acidic OH groups and very strong hydrogen bonds may have Raman shifts below 3000 cm^{-1} . In the studied sample, the two bands at 3594 and 3538 cm^{-1} are assigned to the stretching vibrations of the hydroxyl units. The broad feature of component bands at 2933 and 3170 cm^{-1} reflects vibrations of hydrogen-bonded water molecules in the interlayer space.

Bands of H–O–H ν_2 (δ) bending vibrations of water molecules, occasionally observed in related phosphate minerals in the range 1700–1600 cm^{-1} , were not detected. A similar lack of these manifestations in the Raman spectrum of jasonsmithite is explained as being related to the existence of many different H_2O sites resulting in many overlapping, broad low-intensity peaks not exceeding the background (Kampf et al. 2021).

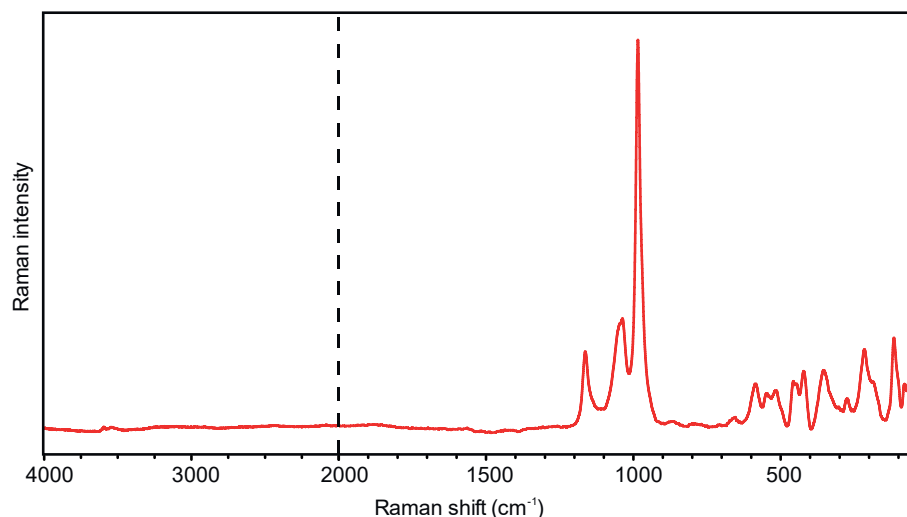


Fig. 3 Full range Raman spectrum of ferraioloite from the Sítio do Castelo mine (split at 2000 cm^{-1}).

Tab. 5 Tentative assignment of Raman spectrum for ferraioloite from the Sítio de Castelo Mine

Wavenumber [cm^{-1}]	<i>FWHM</i> [cm^{-1}]	I_{rel}^*	I_{rel}^{**}	Tentative assignment
3594	16	1	1	ν OH stretching vibrations of the hydroxyl units
3538	60	1	4	
3170	299	1	20	ν OH stretching vibrations of hydrogen-bonded water molecules in the interlayer space
2933	169	1	8	
1163	21	27	31	ν_3 PO_4^{3-} triply degenerate antisymmetric stretching vibrations
1140	28	7	10	
1110	31	4	6	
1052	45	28	68	
1035	25	18	25	
985	14	100	81	ν_1 PO_4^{3-} symmetric stretching vibrations
978	34	53	100	
657	20	2	2	ν_4 (δ) PO_4^{3-} triply degenerate out-of-plane bending vibrations
585	34	17	32	
549	19	10	10	
536	17	6	5	
525	18	5	5	
513	22	13	14	
495	21	6	6	
458	16	17	14	
444	16	14	12	ν_2 (δ) PO_4^{3-} doubly degenerate in-plane bending vibrations
421	26	26	34	
353	42	26	55	M -O stretching O - M -O symmetric bending vibrations lattice vibrations
320	31	10	16	
301	18	7	7	
292	5	2	1	
274	31	17	27	
253	10	2	2	
231	40	18	37	
215	23	25	29	
200	23	12	15	
183	27	21	29	
167	22	11	12	lattice vibrations
147	25	12	15	
133	14	9	7	
116	19	44	43	
100	19	23	23	
80	17	26	24	
61	21	34	38	

* calculated from the band height

** calculated from the band area

In the phosphate P–O stretching region (Frost et al. 2002), the strongest maximum composed of peaks at 985 and 978 cm^{-1} is interpreted as due to ν_1 PO_4 symmetric stretching vibrations (Fig. 4b). Less distinct bands at 1052 and 1035 cm^{-1} , as well as at 1163, 1140 and 1110 cm^{-1} , are attributed to ν_3 PO_4 triply degenerate antisymmetric stretching vibrations. With PO_4 vibrations, ZnO_4 vibrations may overlap in this region (Kampf et al. 2021).

A series of peaks with gradually increasing intensity appears in the wavenumber region below 700 cm^{-1} . This interval is shown in Fig. 4c and Fig. 4d. As regards the PO_4 unit, two groups of overlapping bands in Fig. 4c can be assigned to (i) ν_4 (δ) PO_4 triply degenerate out-of-plane bending vibrations (657–495 cm^{-1}) and (ii) ν_2 (δ) PO_4 doubly degenerate in-plane bending vibrations (458–421 cm^{-1}). In the first-mentioned group, δ M -O bending vibrations most likely occur and overlap the PO_4 bands. The weak band observed at 657 cm^{-1} could be assigned to water libration modes, although the band position for the libration modes might be expected at higher wavenumbers (Frost et al. 2010).

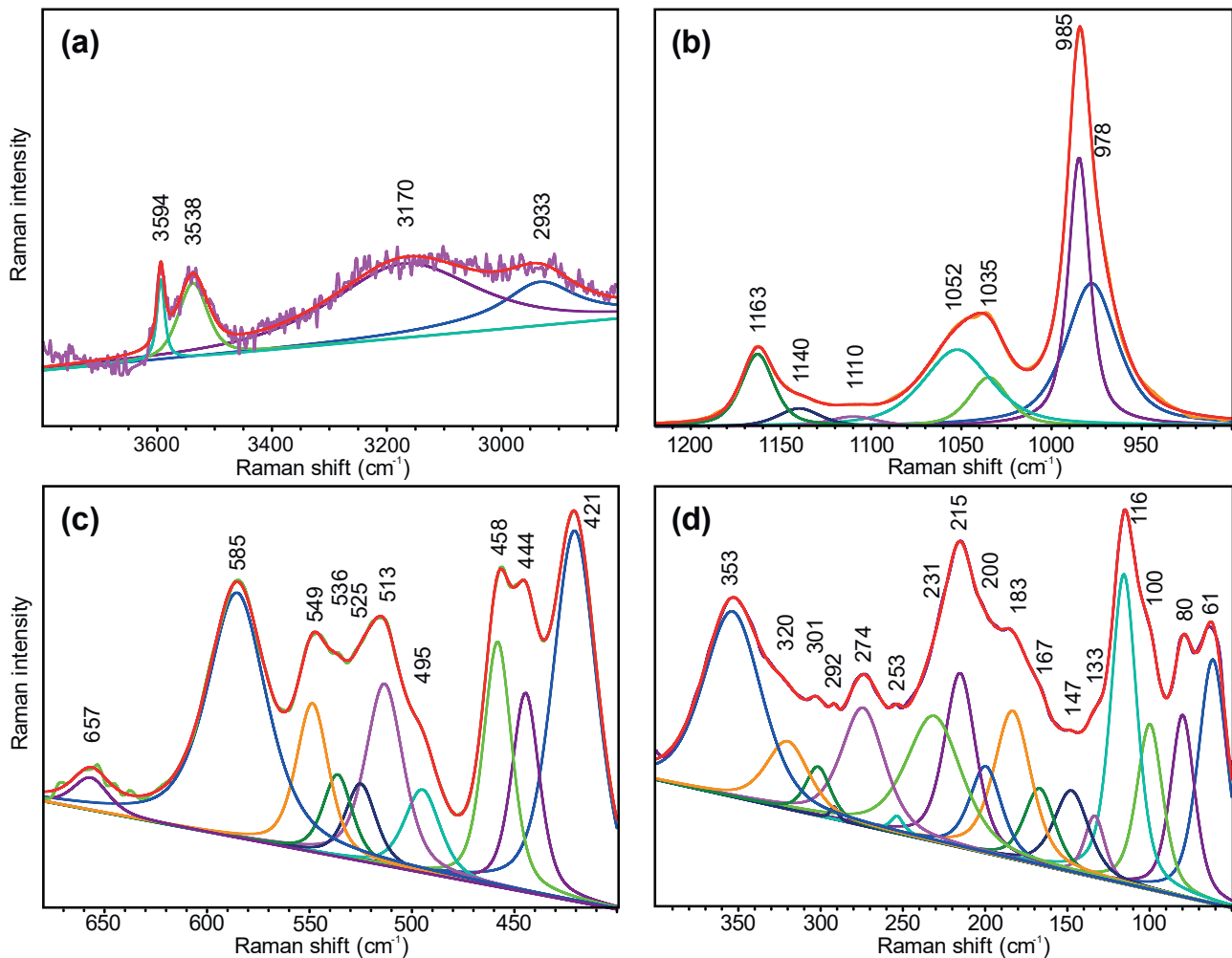


Fig. 4a–d Results of the band component analysis in the Raman spectrum.

In the low wavenumber region (Fig. 4d), bands attributed to vibrations of complex metal-centered polyhedra are shown. Bands of $M-O$ stretching (most likely at 353–253 cm^{-1}) overlap there those of $O-M-O$ symmetric bending (most likely at 231–200 cm^{-1}) vibrations. The bands at lower wavelengths belong to external or lattice vibrations, but some can probably overlap to the range of higher wavenumbers. The band assignment in this spectral region is not entirely clear. For example, an intense band at 215 cm^{-1} observed in the bobierite pattern is attributed to the $Mg-O$ stretching vibration (Frost et al. 2002), and conversely, bands below 249 cm^{-1} in pseudolaueite are considered to be lattice modes (Frost et al. 2015).

7. Note on the origin

Alves et al. (2012) pointed out the similarity of the phosphate occurrence in the Sítio do Castelo mine with those at the Krásno deposit in the Czech Republic (Sejkora et al.

2006). Characteristic primary phosphates at both localities are triplite and zwieselite, which were locally transformed to the isokite-fluorapatite mixture by metasomatic action of alkali-rich fluids in an early hydrothermal stage. The same solutions probably contained metals, including zinc, which resulted in the formation of sphalerite.

During late hydrothermal to supergene stages, extensive alteration led to leaching and redeposition of chemical components. In corrosion cavities in primary phosphates and on nearby and more distant fissures, a diverse suite of secondary minerals subsequently crystallized, containing additional elements introduced by circulating aqueous solutions. The studied ferraiolite is one of the youngest minerals in the locality. Considering that its occurrence is limited to an area only a few centimeters wide, the conditions for its formation had to be very specific. The mineral probably crystallized from alkaline solutions enriched in Al from aluminosilicates, and Zn, Ca and Mg from sphalerite-rich fluorapatite–isok-

ite assemblages in the Fe- and Mn-rich zwieselite–triplite environment.

8. Conclusions

Despite the expectation of Mills et al. (2016) to be found more often in other phosphate-bearing localities, the here described Zn-phosphate from Sítio do Castelo mine seems to be the second known occurrence of ferraioloite. The studied sample shows specific differences compared to the type specimen from the Foote mine, USA, especially in the low content of Mg and a significant proportion of Na in the interlayer sites. Because it was impossible to obtain the data needed to determine the site's site occupancy in the mineral's crystal structure, we report the studied mineral phase as sodium-rich ferraioloite with large cations in the interlayer.

Acknowledgments. The authors wish to express their thanks to Jakub Plášil (Institute of Physics ASCR, Prague) for his kind support in this study, and Alexandre Lima (Departamento de Geociências, Ambiente e Ordenamento do Território, University of Porto) for information regarding the locality. Anthony R. Kampf, Ian E. Grey and Jan Cempírek are acknowledged for valuable comments and suggestions improving the manuscript. This work was supported financially by the Ministry of Culture of the Czech Republic (long-term project DKRVO 2019-2023/1.II.c National Museum, 00023272).

References

- ALVES P, LEAL GOMES C, LOPES NUNES JE (2012) Produtos de evolução de triplite-zwieselite, fluorapatite e isokite da mina Sítio do Castelo (Folgosinho, Guarda). II Congresso Jovens Investigadores em Geociências, LEG 2012, 1–4
- ALVES P, VIÑALS J, REWITZER C, VILA F, MEISSER N (2016) Folgosinho: Secondary phosphates from the Sítio do Castelo mine - Gouveia, Guarda, Portugal. *Mineral up* 4: 6–27
- BURNHAM CW (1962) Lattice constant refinement. *Carnegie Inst. Washington Year Book* 61: 132–135
- CHUKANOV NV, VIGASINA MF (2020): Vibrational (infrared and Raman) spectra of minerals and related compounds. Springer Nature Switzerland, pp 1–1255
- FROST RL, MARTENS W, WILLIAMS PA, KLOPROGGE JT (2002) Raman and infrared spectroscopic study of the vivianite-group phosphates vivianite, baricite and bobierite. *Mineral Mag* 66: 1063–1073
- FROST RL, SEJKORA J, KEEFFE EC, PLÁŠIL J, ČEJKA J, BAHFENNE S (2010) Raman spectroscopic study of the phosphate mineral churchite-(Y) $\text{YPO}_4 \cdot 2\text{H}_2\text{O}$. *J Raman Spectrosc* 41: 202–206
- FROST RL, SCHOLZ R, WANG L (2015) A Raman and infrared spectroscopic study of the phosphate mineral pseudolaueite and in comparison with strunzite and ferrostrunzite. *J Chem Crystallogr* 45: 391–400
- GARATE-OLABE I, RODA-ROBLES E, GIL-CRESPO PL, PÉREZ A, VIEIRA R, LIMA A (2012) Estudio textural y mineralógico del dique de cuarzo con fosfatos de Folgosinho (Guarda, Portugal). *Macla* 16: 220–221
- GREY IE, KAMPF AR, KECK E, MACRAE CM, CASHION JD, GOZUKARA Y (2018) Crystal chemistry of schoonerite-group minerals. *Eur J Mineral* 30: 621–634
- KAMPF AR, MILLS SJ, SIMMONS WB, NIZAMOFF JW, WHITMORE RW (2012) Falsterite, $\text{Ca}_2\text{MgMn}^{2+}_2(\text{Fe}^{2+}_{0.5}\text{Fe}^{3+}_{0.5})_4\text{Zn}_4(\text{PO}_4)_8(\text{OH})_4(\text{H}_2\text{O})_{14}$, a new secondary phosphate mineral from the Palermo No. 1 pegmatite, North Groton, New Hampshire. *Amer Miner* 97: 496–502
- KAMPF AR, GREY IE, ALVES P, MILLS SJ, NASH BP, MACRAE CM, KECK E (2017) Zincostrunzite, $\text{ZnFe}^{3+}_2(\text{PO}_4)_2(\text{OH})_2 \cdot 6.5\text{H}_2\text{O}$, a new mineral from the Sítio do Castelo mine, Portugal, and the Hagendorf-Sud pegmatite, Germany. *Eur J Mineral* 29: 315–322
- KAMPF AR, CELESTIAN AJ, NASH BP (2021) Jasonsmithite, a new phosphate mineral with a complex microporous framework, from the Foote mine, North Carolina, U.S.A. *Amer Miner* 106: 174–179
- MILLS SJ, GREY IE, KAMPF AR, MACRAE CM, SMITH JB, DAVIDSON CJ, GLENN AM (2016) Ferraioloite, a new secondary phosphate mineral from the Foote mine, USA. *Eur J Mineral* 28: 655–661
- NAKAMOTO K (2009) Infrared and Raman spectra of inorganic and coordination compounds. Part A: Theory and applications in inorganic chemistry. John Wiley & Sons, Inc., Hoboken, New Jersey, pp 1–419
- ONDRUŠ P (1993) ZDS – A computer program for analysis of X-ray powder diffraction patterns. *Materials Science Forum* 133–136, 297–300, EPDIC-2. Enschede
- POUCHOU J, PICHOU F (1985) „PAP“ ($\phi\rho z$) procedure for improved quantitative microanalysis. In: ARMSTRONG JT (ed): *Microbeam Analysis*: 104–106. San Francisco Press. San Francisco
- SEJKORA J, ŠKODA R, ONDRUŠ P, BERAN P, SÜSSER C (2006) Mineralogy of phosphate accumulations in the Huber stock, Krásno ore district, Slavkovský les area, Czech Republic. *J Czech Geol Soc* 5: 103–147
- TEIXEIRA C, BRITO DE CARVALHO LH, PAULA SANTOS J, MARTINS PERES A, DE BARROS RF, PILAR L, PEINADOR FERNANDES A, TAVARES ROCHA A (1967) Carta geológica de Portugal na Escala de 1/50000. Folha 17-D Gouveia. Serviços geológicos de Portugal, Lisboa
- YVON K, JEITSCHKO W, PARTHÉ E (1977) Lazy Pulverix, a computer program for calculation X-ray and neutron diffraction powder patterns. *J Appl Crystallogr* 10: 73–74